

# Equivalent viscous damping of SMA bar connectors in post-tensioned segmental bridge Piers



**H. Roh and J.S. Lee**

*Hanyang University, Korea*

**A.M. Reinhorn**

*University at Buffalo-The State University of New York, USA*

## **SUMMARY:**

This study investigates an equivalent viscous damping (EVD) ratio of the post-tensioned piers when the Shape Memory Alloy (SMA) bars are used. Two types of large diameter NiTi SMA bars are considered, a 25.4mm diameter superelastic bar and a 36.5mm diameter martensitic bar. Both are designed to be 1% of the gross column sectional area. Two slenderness ratios (length/depth) for the segmental piers are considered, namely 7.5 and 5.0. Modelling details such as a moment-curvature relationship for the piers and a modified four-spring model for the SMA bars are presented. A cyclic response analysis is conducted increasing the lateral drift ratio to 6%. When the martensitic SMA bars are used, the EDV ratio of between 10.5% and 12.5% is obtained for the piers with different slenderness ratios under the post-tensioning forces as much as 50% of the tendon's yield stress. However, the damping ratio of the piers connected with the superelastic SMA bars is considerably lower and between 5% and 7%.

*Keywords: Segmental rocking piers, Energy dissipation, SMA bar connectors*

## **1. INTRODUCTION**

Many studies have been conducted to identify and/or increase the energy dissipation capacity of PT segmental columns by using special yielding devices (Wang et al. 2008; Sideris et al. 2010; ElGawady and Sha'lan 2011). In the present study, nitinol (NiTi) martensitic Shape Memory Alloys (SMAs) are considered to investigate their contribution to the energy dissipation capacity of the columns. NiTi alloy is the most common type of SMA. Well known material features of the NiTi martensitic SMAs are an excellent performance against corrosion and the shape memory effect which is the ability to recover their original shape by heating, even though the SMA bars have a residual stress at zero strain during cyclic behavior (Ocel et al. 2004). Recently, large diameter-bar type of SMAs has been applied to protect civil structures against earthquake events through retrofitting (Effendy et al. 2006; Saiidi et al. 2009; Alam et al. 2012), exploiting their uniaxial stress-strain cyclic characteristics. Compared with the wire type of SMAs, the bar type of SMAs can resist in both the tension and compressive stains. In this paper, cyclic modeling techniques of the PT columns with the NiTi martensitic SMA bars as energy dissipating (ED) bars are presented and the energy dissipation and damping capacity of such columns is compared to that of columns enhanced with the NiTi superelastic SMA bars. For more extensive comparisons, two different slenderness ratios are considered for the columns, representing slender and medium size columns.

## **2. PT COLUMN DESIGN WITH NITINOL MATERNSITIC SMA BARS**

The column configuration considered in this study is presented in Fig. 2.1, which is post-tensioned with a tendon located at the centerline of the column. The PT tendon is left unbonded with the surrounding concrete and provides the clamping force required to hold the column segments together. This study assumes that the joints of the segments are strongly tied to each other. Such connections

provide an identical behavior to the one of single rocking columns presented in the references (Mander and Cheng 1997; Palermo et al. 2005; Roh 2007), and named segmental rocking columns in this paper. Concrete shear keys are used at the segment joints to prevent sliding and to transfer the shear force completely. Another column specimen with different slenderness ratio of 5 defined as  $L'/d_c$  are considered, where,  $L'$  is the column length and  $d_c$  is the column depth. The specimen is designed with a height of 6.0m and is made of six blocks of 1.0m each. The edges at the base of the column are cut 50mm deep and 5mm in height, so that with a rotational angle below 1/10rad, corresponding to a rotational drift ratio of 10%, the cut surfaces do not come in contact with the foundation, thus the cut surfaces do not interrupt the lateral behavior of the column. Such shallow or spherical cut edges lead to a nonlinear elastic-cyclic curve of the segmental rocking columns, due to minimized stress concentration and crushing in that area. Similar results are found in Besa et al. (2010) and Roh and Reinhorn (2010a).

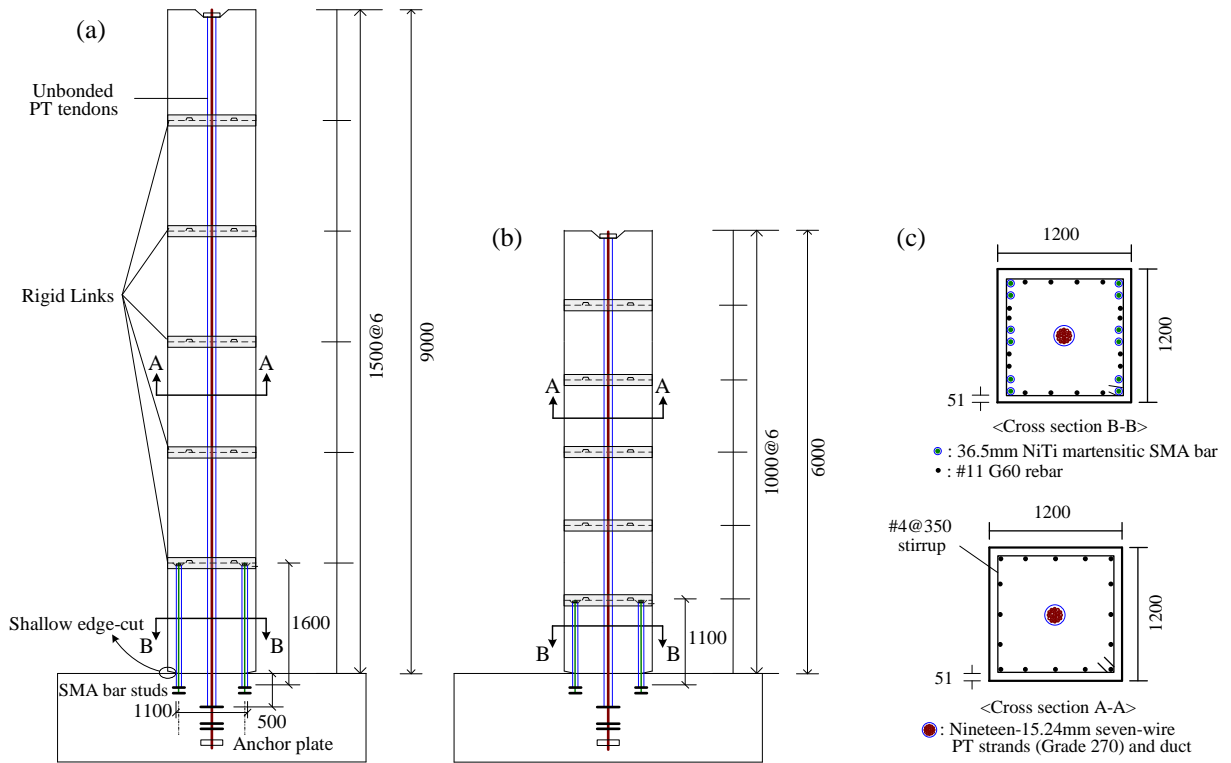


**Figure 2. 1.** Segmental column: (a) 7.5 of slenderness ratio (adapted from Roh and Reinhorn, 2010b), (b) 5.0 of slenderness ratio, and (c) reinforcements for sections A-A and B-B (unit: mm)

For the material properties, the compressive strength of concrete,  $f'_c$ , is 40MPa and the corresponding yield strain is 0.0013. The longitudinal reinforcement consists of #11 rebar as shown in Fig. 2.1(c) and the reinforcement ratio is 1.12% of the cross section area ( $A_g = d_c t$ ), where,  $t$  is the width of the columns. The yield stress of the PT tendon is 1690MPa and its ultimate stress specified in ASTM A416 is 1860MPa (G270). The post-tensioning force level applied to the tendons is taken equal to 50% of the yield strength. The PT tendon is designed with nineteen 15.24mm diameter seven-wire strands (strand designation no. 15) presented in ASTM A416. The total area of the tendon is 2660 mm<sup>2</sup>, which is 0.22% of the cross sectional area of the column. The nominal strength of the column is defined here as  $N_0 = f'_c A_g$  (48400kN). The specified gravity load due to the bridge deck ( $W_{Deck}$ ) is 5% of the nominal strength, which is 2420kN. As shown in Fig. 2.1, the SMA bars are provided in the base segment only. The 25.4mm diameter superelastic and 36.5mm diameter NiTi martensitic SMA bars considered in this study were tested by McCormick and DesRoches (2004); their test results are shown in Fig. 3.1. The loading rate applied was 0.025 Hz which yields a quasi-static behavior. The obtained elastic modulus of the martensitic and superelastic SMA bars is about 38GPa and 28GPa,

respectively. The yield stresses of the martensitic bar are 180MPa and 280MPa for a tensile and compressive behaviour, respectively, while the yield stress of the superelastic bar is 380MPa. In this study, the ED bar ratio is designed to be 1%. More details about the material properties and experiment can be found in the reference (McCormick and DesRoches 2004).

### 3. MODELING DETAILS

The segmental rocking columns are modeled using the numerical platform developed by Roh and Reinhorn (2009, 2010a) and implemented in IDARC2D (Reinhorn et al. 2009). The model was developed based on the flexibility matrix approach using the sectional moment-curvature relationship of the rocking columns. Other computational techniques are coupled, such as the nonlinear elastic-cyclic rules, the modified spread plasticity model, and the stepwise strength reduction schemes simulating the apparent negative stiffness range (post-rocking range). The definitions of the moment-curvature and the complementary tools are found in Roh and Reinhorn (2010a). The PT tendon is modeled by a bilinear elastic-plastic spring.

The behavior of the SMA bars is modelled by a combination of four springs. Such way was introduced by Roh and Reinhorn (2010b) for a superelastic SMA bar, modifying the existing smooth hysteretic model (SHM) proposed by Sivaselvan and Reinhorn (2000). In the four-spring model, Spring 1 represents the post-yield stiffness which models the phase transformation of the SMA bar. The plain hysteretic behavior is modeled using Spring 2. Simultaneously, Spring 3 representing a slip-lock behavior operates during unloading only (reverse phase transformation region) and Spring 4 is a gap-closing stiffness which is intended to model the transition between the plateau and the martensitic region. The stiffness of the gap spring is constant when the SMA bar shows a pure martensitic behavior. The formulation of the model is summarized below:

$$\text{Spring 1: } E_{\text{post-yield}} = \alpha_1 E_0, \quad (3.1)$$

$$\text{Spring 2: } E_{\text{hysteretic}} = (R_K - \alpha_1) E_0 \left\{ 1 - \left| \frac{\sigma^*}{\sigma_y^*} \right|^{N_{\text{hys}}} \left[ \eta_1 \text{sgn}(\sigma^* \dot{\varepsilon}) + 1 - \eta_1 \right] \right\} \quad (3.2)$$

$$\text{Spring 3: } E_{\text{slip-lock}} = \left\{ \sqrt{\frac{2}{\pi}} \frac{|s|}{|\sigma_\omega^*|} \exp \left[ -\frac{1}{2} \left( \frac{|\sigma^*| - |\lambda \sigma_y^*|}{\omega \sigma_y^*} \right)^2 \right] \right\}^{-1} \quad (3.3)$$

$$\text{Spring 4: } E_{\text{gap-closing}} = (\alpha_2 - \alpha_1) E_0 \left[ \left( \frac{|\varepsilon| - |\varepsilon_{\text{gap}}|}{|\mu \varepsilon_{\text{gap}}|} \right)^{N_{\text{gap}} - 1} \times \right. \\ \left. U(|\varepsilon| - |\varepsilon_{\text{gap}}|) U(-|\varepsilon| + |\varepsilon_m|) + U(|\varepsilon| - |\varepsilon_m|) \right] \quad (3.4)$$

For the evaluation of the total stiffness ( $E_s$ ), the hysteretic and slip-lock springs are obtained by using the fourth order Runge-Kutta (RK) method and combined in series. The post-yielding and gap-closing springs are then simply added to the result of the series combination. The hysteretic control parameters of the martensitic and superelastic SMA bar specimens used for in the numerical simulation applied to the four-spring model are presented in Table 3.1. The same loading protocol applied by McCormick and DesRoches (2004) is used for the simulation of the SMA bar specimens. Fig. 3.1(b) and (d) show how the simulation results appear in good agreement with those obtained by the test results of the SMA bars (McCormick and DesRoches, 2004). Even though on the compressive strain side of the martensitic bar the strength variation does not match well, the present model can be acceptable since the SMA bars installed in the PT columns work only in tensile strain.

**Table 3.1.** Hysteretic control parameters of martensitic and superelastic SMA bars

	36.5mm dia. NiTi martensitic SMA bars	25.4mm dia. NiTi superelastic SMA bars (Roh and Reinhorn 2010b)
$\alpha_1$	0.118	0.076
$\alpha_2$	-	0.25
$\varepsilon_y^+$	0.0047	0.0139
$\varepsilon_y^-$	-0.0068	-
$\varepsilon_{gap}$	0.055	0.04
$\varepsilon_m$	-	0.06
$N_{hys}$	5.0 for first and third quadrants	5.0
	0.5 for second quadrant	
	0.8 for fourth quadrant	
$N_{gap}$	-	2.2
$\eta_1$	0.5	0.0 for $ \varepsilon  < \varepsilon_y$
		0.5 for $ \varepsilon  \geq \varepsilon_y$
$\alpha$	50	200
$s$	0.045	Variable (Roh and Reinhorn, 2010b)
$\lambda$	0.83	0.401
$\omega$	0.05	0.125
$\mu$	-	0.33

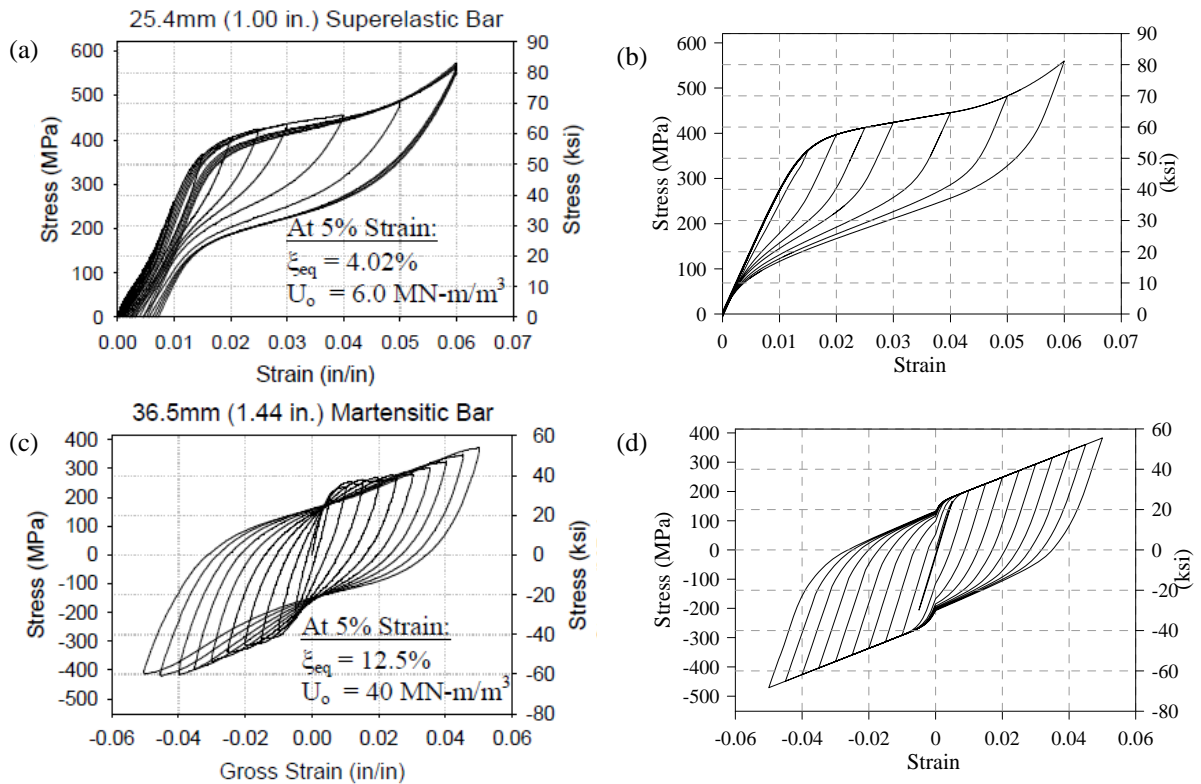


**Figure 3. 1.** Quasi-static cyclic-uniaxial strain curves: (a) test result (McCormick and DesRoches, 2004) and (b) numerical simulation for superelastic SMA bars, (c) test result (McCormick and DesRoches, 2004) and (d) numerical simulation for martensitic SMA bars

#### 4. CYCLIC RESPONSES AND DAMPING CAPACITY

The cyclic response of the segmental rocking columns is shown in Fig. 4.1 in terms of the force-base rotation angle relation which is almost the same as the lateral drift ratio. The loading protocol applied to the specimens consists of increasing lateral displacement cycles of 0.5%, 1%-6% drift with increments of 1% drift ratio. The cyclic responses of the column using the superelastic and martensitic SMA bars show a flag shape hysteretic behavior and a high ductile behavior. However, there is no residual drift or rotation. Compared to the 7.5-slenderness segmental rocking column, the lateral strengths of the 5.0-slenderness column are considerably increased for both the superelastic and martensitic bar applications. In the application of the martensitic SMA bars as shown in Fig. 4.1(a), the strength increment of the 5.0-slenderness ratio is almost 90%, compared to the 7.5-slenderness ratio. Similar results are found in the application of the superelastic SMA bars as shown in Fig. 4.1(b). This is due to the reduced column length (stiffer) and larger strain behavior of the SMA bars and PT tendons. The PT tendon is slightly yielded when the column slenderness ratio is reduced to 5.0; however, the tendon does not yield much and is able to provide a restoring force big enough to allow for no residual drift. However, the tendon yielding slightly affects on the lateral strength of the columns at the large drift ratio (4%-6%).

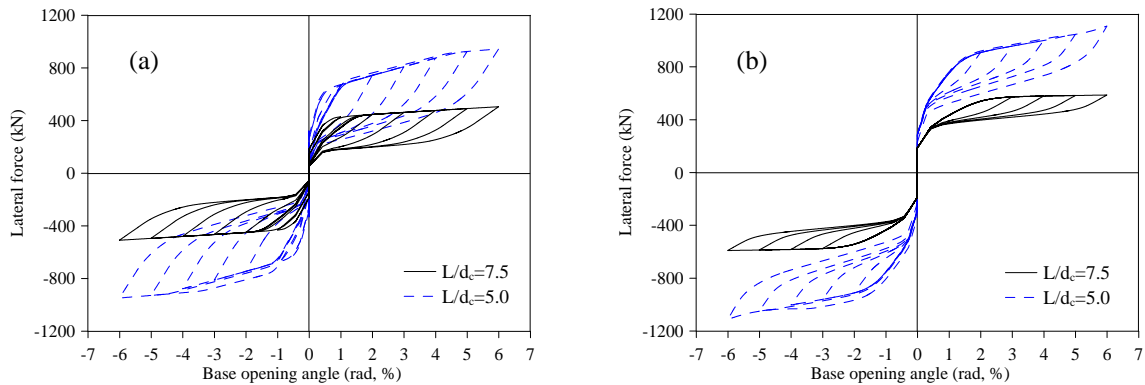


**Figure 4. 1.** Cyclic response of the PT columns: (a) martensitic bars and (b) superelastic bars

The dissipated energy and equivalent viscous damping ratio are presented in Figs. 4.2 and 4.3. The use of the martensitic SMA bars provides more energy dissipation. Reducing the column slenderness ratio to 5.0 leads to the increase of the amount of the energy dissipation. For the 7.5-slenderness ratio as shown in Fig. 4.2(b), the axial stress of the superelastic SMA bars does not reach the yield stress until base rotations of 2%, thus no energy dissipation from the SMA bars occurs before such rotations. When the length of the superelastic SMA bars is reduced ( $L/d_c=5.0$ ), the axial stress-strain behavior of the bars is activated more and yielding is reached for base rotations that are lower than 2%; thus the SMA bars provide energy dissipation. From 5% drift ratio which the tendon starts to yield, the amount of dissipated energy becomes larger, compared to the case of 7.5- slenderness ratio.

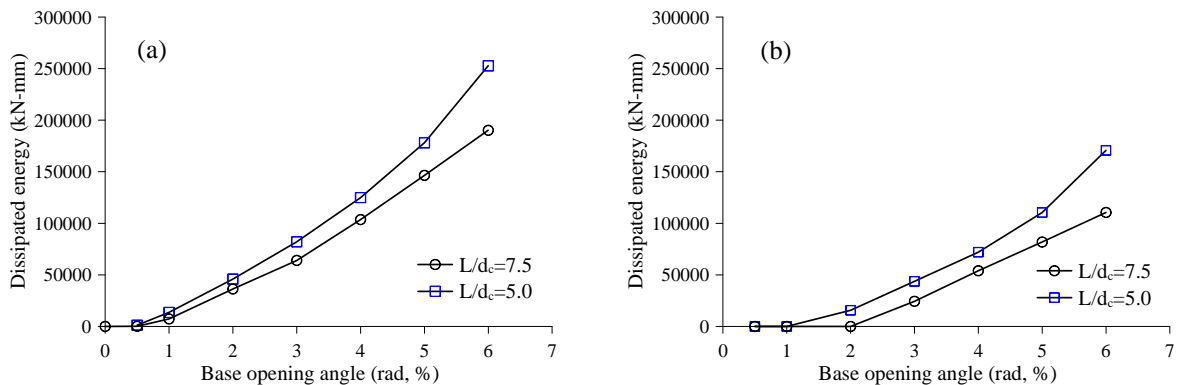


**Figure 4. 2.** Dissipated energy variations of the PT columns: (a) martensitic bars and (b) superelastic bars

When the martensitic SMA bars are used as shown in Fig. 4.3(a), the equivalent damping ratio of the case  $L/d_c = 7.5$  is smaller than that when the  $L/d_c = 5.0$  is used, but it becomes closer at the large drift. Therefore, the effect of the column slenderness on the damping ratio becomes small. At 6% rotational drift, the damping ratio for the case of 7.5 slenderness increases to about 11%. The damping ratio of the 5.0-slenderness column specimen increases rapidly to ~8% even for small rotational drifts up to 2%. Thereafter the damping ratio increases consistently. Overall, when the martensitic SMA bars are, the damping ratio is about 10.5%~12.5% at 6% rotational drift, while the columns using the superelastic SMA bars provide a damping ratio of about 5%~7% at the same rotational drift as shown in Fig. 4.3(b).

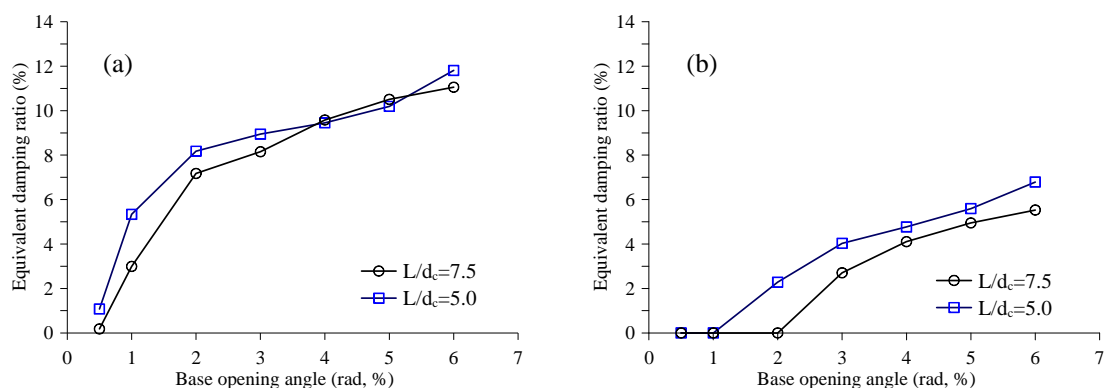


**Figure 4. 3.** Equivalent damping ratio of the PT columns: (a) martensitic bars and (b) superelastic bars

## 5 CONCLUSIONS

This paper presents quasi-static cyclic modeling techniques for PT segmental rocking columns connected with the NiTi SMA bars at their base and their damping capacity is investigated through cyclic analyses. Compared to the 7.5-slenderness column, the column with a slenderness of 5.0 provides much higher lateral resistance. Also the column activates more the tensile strain behavior of the SMA bars and PT tendons; thus the dissipated energy and damping ratio is increased even at small displacements. However, at large displacements, the damping ratio becomes closer to that of the 7.5-slenderness column because the corresponding lateral strength is also increased. When the martensitic SMA bars are used, an equivalent viscous damping ratio is obtained with values between 10.5% and 12.5% (at 6% rotational drift). When the superelastic SMA bars are used to provide energy dissipation, the damping ratios are only about 5% -7%. These values are almost half of those resulting from the use of the martensitic SMA bars.

## ACKNOWLEDGMENTS

This work was supported by the research fund of Hanyang University (HY-2010-N).

## REFERENCES

- Alam, M.S., Moni, M. and Tesfamariam, S. (2012). Seismic overstrength and ductility of concrete buildings reinforced with superelastic shape memory alloy rebar. *Engineering Structures* **34:1**, 8-20.
- Besa, J., de la Llera, J.C. and Jünemann R. (2010). Experimental behavior and design of a new kinematic isolator. *Engineering Structures*, **32:2**, 508-522.
- Effendy, E., Liao, W.I., Song, G., Mo, Y.L. and Loh, C.J. (2006). Seismic behavior of low-rise shear walls with SMA bars. *Proceedings of Earth & Space 2006: Engineering, Construction, and Operations in Challenging Environments*.

- ElGawady, M.A. and Sha'lan, A. (2011). Seismic behavior of self-centering precast segmental bridge bents. *Journal of Bridge Engineering* **16:3**, 328-339.
- McCormick, J. and DesRoches, R. (2004). Damping properties of shape memory alloys for seismic applications. *2004 Structures Congress*, 1-11.
- Mander, J.B. and Cheng, T.T. (1997). Seismic Resistance of Bridge Piers Based on Damage Avoidance Design. Technical Report NCEER 97-0014, University at Buffalo, The State University of New York.
- Ocel, J., DesRoches, R., Leon, R.T., Hess, W.G., Krumme, R. and Hayes, J.R. (2004). Steel beam-column connections using shape memory alloys. *Journal of Structural Engineering* **130:5**, 732-740.
- Palermo, A., Pampanin, S. and Calvi, G.M. (2005). Concept and development of hybrid solutions for seismic resistant bridge systems. *Journal of Earthquake Engineering* **9:6**, 899-921.
- Reinhorn, A.M., Roh, H., Sivaselvan, M., Kunnath, S.K., Valles, R.E., Madan, A., Li, C., Lobo, R. and Park, Y.J. (2009). IDARC2D version 7.0: A program for the inelastic damage analysis of structures. Technical Report MCEER-09-0006, University at Buffalo, The State University of New York.
- Roh, H. (2007). Seismic Behavior of Structures using Rocking Columns and Viscous Dampers. Ph.D. Dissertation, University at Buffalo, The State University of New York.
- Roh, H. and Reinhorn, A.M. (2009). Nonlinear static analysis of structures with rocking columns. *Journal of Structural Engineering* **136:5**, 532-542.
- Roh, H. and Reinhorn, A.M. (2010a). Modeling and seismic response of structures with concrete rocking columns and viscous dampers. *Engineering Structures* **32:8**, 2096-2107.
- Roh, H. and Reinhorn, A.M. (2010b). Hysteretic behavior of precast segmental bridge piers with superelastic shape memory bars. *Engineering Structures* **32:10**, 3394-3403.
- Saiidi, M.S., O'Brien, M. and Sadrossadat-Zadeh, M. (2009). Cyclic response of concrete bridge columns using superelastic nitinol and bendable concrete. *ACI/Structural Journal* **106:1**, 69-77.
- Sideris, P., Anagnostopoulou, M., Aref, A. and Filiatrault, A. (2010). Seismic performance of precast segmental bridges. *9th US national and 10th Canadian Conference on Earthquake Engineering*, Paper # 1499.
- Sivaselvan, M.V. and Reinhorn, A.M. (2000). Hysteretic models for deteriorating inelastic structures. *Journal of Engineering Mechanics* **126:6**, 633-640.
- Wang, J.C., Ou, Y.C., Chang, K.C. and Lee, G.C. (2008). Large scale seismic tests of tall concrete bridge columns with precast segmental construction. *Earthquake Engineering and Structural Dynamics* **37:12**, 1449-1465.